Three-Dimensional Natural Convection Experiments in an Enclosure

D. Sadowski,* D. Poulikakos,† and M. Kazmierczak*
University of Illinois at Chicago, Chicago, Illinois

This paper presents an experimental investigation for the phenomenon of three-dimensional natural convection inside a rectangular cavity driven by a single vertical wall with a warm and a cold region. The warm and the cold regions on this wall were located side-by-side. The remaining walls are adiabatic. The experiments focus on the high Rayleigh number regime ($3 \times 10^9 < Ra < 5 \times 10^{10}$). Apart from the region near the vertical driving wall and along the adjoining top and bottom surfaces close to the driving wall, the temperature field is remarkably two-dimensional, linearly stratified in the vertical direction. The fluid in the remainder of the enclosure is practically stagnant. The flow, wherever it exists, is laminar except for two small local turbulent regions near the top and bottom corners of the driving wall. Heat transfer results are correlated by $Nu = 0.031 \times Ra^{0.324}$. The study is concluded with a scaling analysis which aims to explain in a fundamental sense the experimental findings.

Nomenclature

c_p = specific heat, J/kg K
$f(Ra)$ = function of Rayleigh number, Eq. (19)
g = gravitational acceleration, m/s^2
H = height of the enclosure, m
k = thermal conductivity, W/mK
L = length of the enclosure, m
Nu = Nusselt number, Eq. (1)
P = pressure, N/m^2
P_b = power dissipated by bottom heater, W
P_t = power dissipated by top heater, W
Q = heat transfer rate, W, Eq. (1)
Ra = Rayleigh number, Eq. (2)
T_C = cold wall temperature, K
T_H = hot wall temperature, K
ΔT = temperature difference between cold and hot walls, K
u = vertical velocity component, m/s
v = horizontal velocity component, m/s
W = width of the enclosure, m
x = vertical coordinate, m
y = horizontal coordinate, m
α = thermal diffusivity, m^2/s
β = coefficient of volumetric thermal expansion, K^{-1}
δ_t = thermal boundary layer thickness, m
ν = kinematic viscosity, m^2/s
θ = temperature scale of the core region, K
ϕ = temperature scale of the bottom layer of fluid, K
ρ = density, kg/m^3

Subscripts

o = reference state
in = into the system
out = out of the system

Introduction

NATURAL convection heat transfer across fluid-filled enclosures has been studied analytically, numerically, and experimentally for the past few decades. Extensive reviews of this work are given by Churchill,[1] Catton,[2] Ostrach,[3] and Bejan.[4] The interest in this field stems from the many engineering applications involving natural convection. These applications include heating and cooling of buildings, the cooling of electronic components, nuclear reactor safety, solar energy collectors, and a host of others.

Most of the basic research on free convection in enclosures has centered on rectangular and cylindrical enclosures, though studies have been reported focusing on triangular,[5] and spherical enclosures.[6] In virtually all of the studies to date on rectangular enclosures, the enclosure has had uniform thermal boundary conditions, i.e., one or more walls with constant heat flux or one or more completely isothermal walls with the remaining walls adiabatic. However, in most applications nonuniform thermal boundary conditions generally exist, and this presents a new class of problems, of which our knowledge is marginal. Pioneering work on free convection from vertical plates with such boundary conditions was done by Sparrow[7] and Schetz and Eichhorn.[8]

More related to our work is Ref. 8, which reports results of natural convection experiments from a vertical plate whose upper half is cold and the lower half warm. More recently, Jaluria[9] examined numerically natural convection from a nonisothermal vertical plate. The flow was induced by isolated thermal sources. The remainder of the plate was adiabatic. The results indicated that the heat transfer from a particular source was affected by the wake of the upstream source.

Only recently has this research been extended to nonuniform thermal boundary conditions on the walls of closed cavities. Chao and his co-workers[10,11] have reported numerical and experimental results for a rectangular enclosure with nonisothermal horizontal walls with applications mainly to solar collectors. Filis and Poulikakos[12] and Poulikakos[13] presented experimental and theoretical studies of free convection in an enclosure with a vertical wall which could be heated on the top half and cooled on the bottom half or vice versa. An experiment for the latter case has also been performed by Humphrey and Bleinc.[14]

This paper addresses the problem of three-dimensional natural convection in a parallelepipedal enclosure having a vertical wall heated on its left half and cooled on its right half. To isolate the effect of this wall the remaining walls are adiabatic. The relation of this work to building heat transfer is clear. In many cases, a single wall of a building is nonisothermal, i.e., it possesses a warm and a cold region. This nonisothermality may be induced by structural reasons (position of windows, doors, heaters, etc.) or by heating of only part of the wall by the sun. The presence of a nonisothermal wall like the one described

Received Feb. 23, 1987; revision received May 26, 1987.

*Graduate Research Assistant, Department of Mechanical Engineering.
†Associate Professor, Department of Mechanical Engineering.

above will affect the air circulation in the building interior. The objective of this research is to determine the natural convection heat transfer and the flow pattern induced in the enclosure by the nonuniform thermal boundary conditions on the wall. Water was the working fluid and the experiment was conducted in the high Rayleigh number regime characteristic of natural convection in buildings, ($3 \times 10^9 < Ra < 5 \times 10^{10}$). The temperature field within the cavity was determined, and flow visualization was achieved by adding neutrally buoyant reflective microdisks to the fluid and passing a sheet of laser light through the enclosure. The study was concluded with a scale analysis which puts into perspective the experimental measurements and observations.

Experimental Apparatus

The experimental apparatus is a rectangular box drawn to scale in Fig. 1. The box has five adiabatic walls of 19 mm thick plexiglass sheet and a driving wall machined from 17.5 mm thick aluminum plate. The inside dimensions of the box are $L = 610$ mm, $H = W = 457$ mm giving a height-to-length aspect ratio of $H/L = 0.749$. The box rests on wooden slats which allows for insulation of the bottom wall. The entire apparatus is insulated with two snugly fitting layers of 51 mm thick styrofoam. The aluminum driving wall is constructed such that half of it may be heated while the other half is cooled. Three electrical strip heaters are mounted on the warm half and the power to each heater is individually controlled by using ac voltage regulators. Each strip heater can dissipate up to 800 W. Even though the apparatus was obviously well insulated, a separate experiment was performed to estimate the heat loss through the plexiglass and aluminum walls to the environment.[12,15] This heat loss was found to be less than 3% of the heat flux provided by the strip heaters. A thin layer of highly conductive silicon paste was applied to the bottom of each heater before it was mounted on the plate. Uniform temperature of the warm region was obtained by applying different voltages across each heater and by relocating a heater if necessary. The final location of the heaters resulted from a trial-and-error procedure. Heat generated electrically on the warm half of the wall passes into the enclosure fluid and is removed by circulating a precooled ethylene glycol and water mixture through a jacket which constitutes the cool half of the driving wall. The inlet temperature of the coolant is held constant to within 0.1°C by using a recirculating refrigerated liquid bath. Using this procedure, each half of the driving wall is made acceptably isothermal (± 1°C). The temperature near the inside surface of the driving wall is monitored with thermocouples. Twenty-one chromel-alumel thermocouples are embedded in the aluminum plate at a distance 1 mm from the inside surface. The thermocouple junction heads are potted in silver epoxy to assure good thermal contact. The thermocouples are arranged in three rows of seven each. Since the temperature of the wall changes from hot to cold over a very small distance compared to the height of the cavity, this represents a good approximation to a "step" change in temperature. The heat conducted through the wall from the warm side to the cool side was minimized by machining a slot 10 mm wide and 13 mm deep between the two sides and filling the slot with Bakelite. To further minimize thermal contact, a 2 mm wide slot was cut through the plate beneath the Bakelite and sealed with a silicon-rubber insulation. The heat transfer by direct conduction from the warm to the cold side through the Bakelite and silicon rubber was found to be negligible and that conducted around the ends of the Bakelite was calculated to be less than 5% of the total heat transfer.

Distilled water is the working fluid in these experiments. As shown in Fig. 1, 45 access ports were drilled in the top wall to allow the insertion of temperature probes. Plexiglass tubes of 3 mm i.d. were inserted into the ports and run through the insulation on the top wall. Thus, temperature measurements can be taken without disturbing the insulation around the box. Windows of insulation can be quickly and easily removed from three side walls and the top wall for photographing the flow within the cavity. This operation has no effect on the study for it lasted only a few minutes, which is very short compared to the time scales of the order of 24 h generally found in enclosure natural convection.

Experimental Procedure

A sequence of steady states was achieved by varying the electrical heat input to the warm side of the driving wall while keeping the coolant temperature constant. The bottom and top heaters supplied most of the power and the middle heater was used only when fine adjustment was necessary. The power supplied by the bottom heater, P_b, and that supplied by the top, P_t, is approximated by $P_b = (1.06P_t + 10.5)$ W. Initially, the heaters were set to provide 100 total W and the coolant was fixed at 12.0°C. The wall temperature was continuously monitored until the warm and cool sides stabilized (about 20 h). The graph of temperature vs height in Fig. 2a shows the isothermality along the vertical centerlines of the hot and cold regions of the driving wall. Figure 2b demonstrates the isothermality

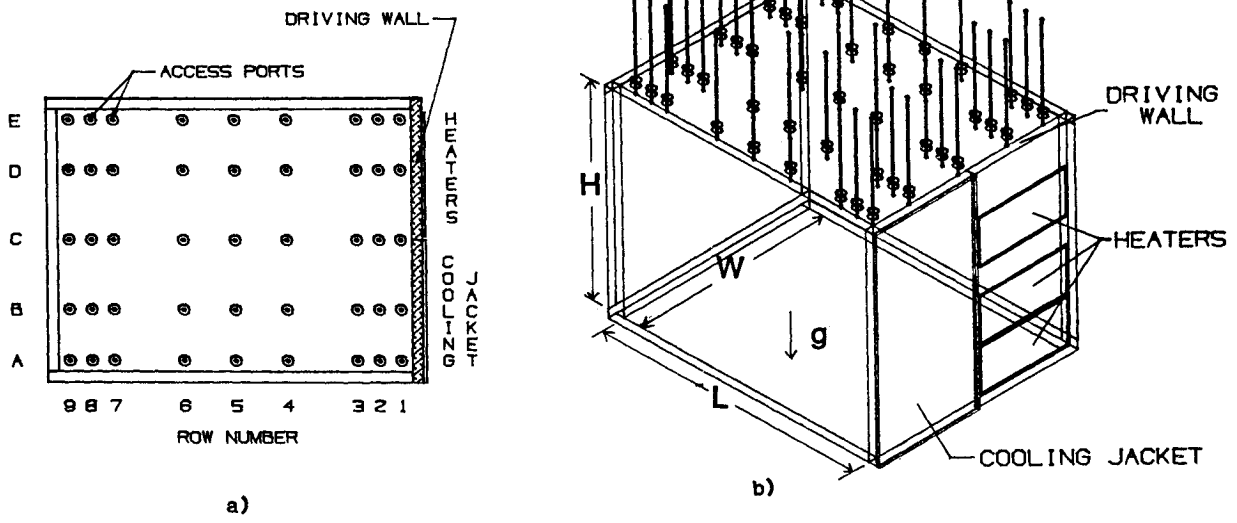

Fig. 1 The experimental apparatus drawn to scale: a) top view, and b) isometric view.

along the horizontal centerline of these regions as well as the step change in temperature between them. The distance indicated in Fig. 2b is measured starting from the edge of the driving wall on the hot side. Wall temperature measurements were taken and averaged arithmetically to obtain T_H and T_C at each steady state. From these we obtained the ΔT $(T_H - T_C)$ needed to calculate the Rayleigh and Nusselt numbers. Next, we increased the heater output by about 75 W and waited 24 h for the next steady state. This continued until the 550-W maximum cooling capacity of the liquid bath was reached. Upon reaching the maximum, the procedure was repeated, but this time reducing the heater output to check for any directional dependence in the experiment. None was found. It is worth clarifying that this procedure tested hysteresis but not necessarily whether the flow pattern in the apparatus was unchanged. While it is true that the core was found to be practically stagnant, weak (hardly detectable) flow patterns may exist and the details of these flow patterns were not examined by this test.

Two representative steady states were chosen for further investigation. The temperature field inside the enclosure was determined when T_H and T_C were approximately equidistant from the ambient room temperature (symmetric case) and when the difference between T_H and ambient temperature was approximately three times the difference between T_C and ambient temperature (asymmetric case). The temperature within the enclosure could be determined at any depth under an access port by a chromel-alumel thermocouple probe of 0.5 mm bead diameter. The probe was constructed by sealing a thermocouple inside a stiff capillary stainless steel tube 0.92 m long. The thermocouple bead was located at one end of the tube and thus came into direct contact with the fluid within the cavity. Five such probes connected to a Hewlett-Packard data acquisition system were used simultaneously. The probes were carefully lowered to a desired depth and held there for 3 min to assure that any flow disturbances had died away. Temperature measurements were taken, and the probes were lowered further until eventually the bottom wall was reached. This procedure was repeated for each of the nine rows of five ports. To insure that the presence of the other four probes was not affecting the readings of the fifth, measurements were taken using only one probe and compared to those obtained when all five probes were present. No differences were found.

In a preliminary study of flow visualization small grains of potassium permanganate were dropped into the cavity through the access tubes. The grains dissolved as they sunk and left a purple trail from the top to the bottom of the tank. The flow was detected by its influence on the trail. We observed strong movement in the top and bottom centimeter of the tank, but the trail through the rest of the cavity was virtually undisturbed. After the grains had set at the bottom for about 30 min the pattern of the flow along the bottom wall could be easily identified. After several observations were made by using the above technique a more accurate method was incorporated to finalize our findings on the flow field.

The second method for visualization of the flowfield was accomplished by adding a rheoscopic suspension of microscopic crystalline disks to the fluid and passing a sheet of laser light through it. The disks are neutrally buoyant and thus have a very large settling time. The concentration of the rheoscopic suspension was 0.1%. The laser sheet was created by passing the beam of a five mW helium-neon laser through a cylindrical lense. Light reflecting off the crystalline disks enabled us to clearly see the general flow pattern within the cavity. Time-exposure photographs were taken of the flow patterns using a Nikon FE 35-mm camera with plus-X ASA 125 black and white film. Many slices of the cavity were examined, but it was readily apparent that all noticeable flow occurred along the driving wall and next to the top and bottom walls only. The core region appeared to be stagnant.

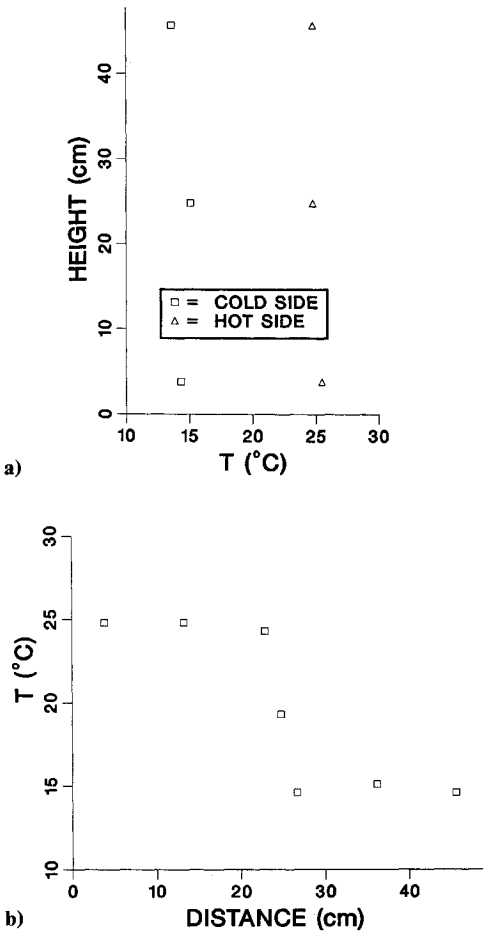

Fig. 2 Temperature profiles showing isothermality of the driving wall: a) vertical isothermality, and b) horizontal isothermality.

Results and Discussion

The temperature field inside the enclosure was determined and detailed temperature measurements were carried out for two representative Rayleigh numbers ($Ra = 2.87 \times 10^{10}$ and $Ra = 4.65 \times 10^{10}$). It was found that the temperature field was qualitatively the same in both cases. Hence, for the sake of brevity, only the temperature results for $Ra = 2.87 \times 10^{10}$ will be reported here. More detailed results are included in Ref. 15.

Figures 3 and 4 report representative temperature variations under selected ports. The location of the ports is shown in Fig. 1. Clearly, near the driving wall (Fig. 3) the temperature is linearly stratified under all ports except for two thin regions in the proximity of the bottom and top walls where the temperature distribution indicates the existence of thermal boundary layers. As we move away from the wall, the thermal boundary layers weaken and finally cease to exist (Fig. 4). Another important result shown in Figs. 3 and 4 is that the three-dimensionality of the temperature field is limited inside the two thin regions near the top and bottom walls. In addition, as we move away from the driving wall (from Fig. 3 to Fig. 4) the three-dimensionality of the temperature fields even inside these thin regions disappears and the temperature field becomes practically two-dimensional (Fig. 4). The steepest temperature variation as we approach the bottom wall is recorded under port 1A where the fluid just leaves the cold portion of the driving wall (Fig. 3). Similarly, the steepest temperature variations as we approach the top wall is recorded under port 1E where the fluid just leaves the warm portion of the driving wall.

To gather further information on the temperature field, extensive measurements were taken and the isotherms shown in Figs. 5 and 6 were constructed. The isotherms in Fig. 5 are for slices perpendicular to the driving wall and parallel to the gravity vector. The temperature field is linearly stratified in the

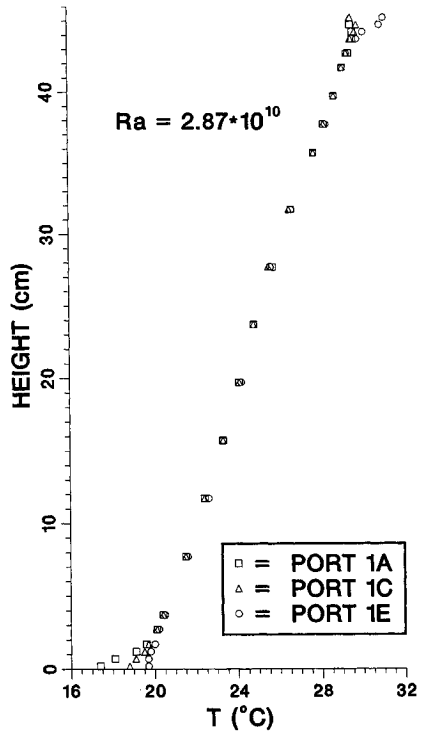

Fig. 3 Vertical temperature profiles for $Ra = 2.87 \times 10^{10}$ under ports 1A, 1C, and 1E.

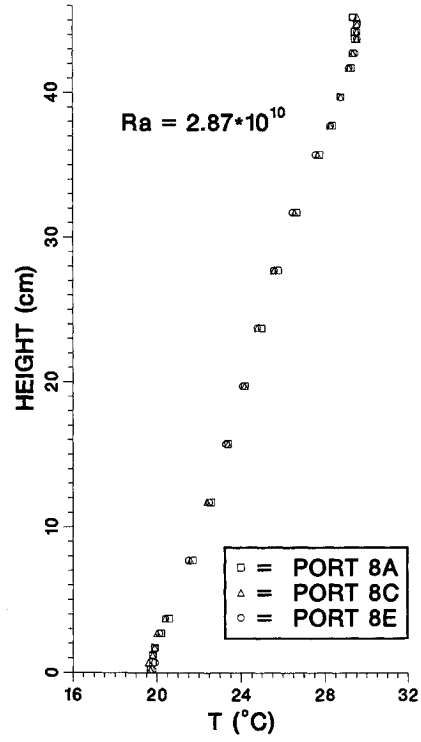

Fig. 4 Vertical temperature profiles for $Ra = 2.87 \times 10^{10}$ under ports 8A, 8C, and 8E.

vertical direction and practically independent of the distance away from this wall except for a thin region near the driving wall where sharp thermal boundary layers exist. The slice perpendicular to the hot part of the aluminum wall (Fig. 5c) shows the existence of a region of warm fluid along the top wall. This fluid region is the continuation of the warm fluid jet traveling upward along the heated portion of the driving wall. Figure 6

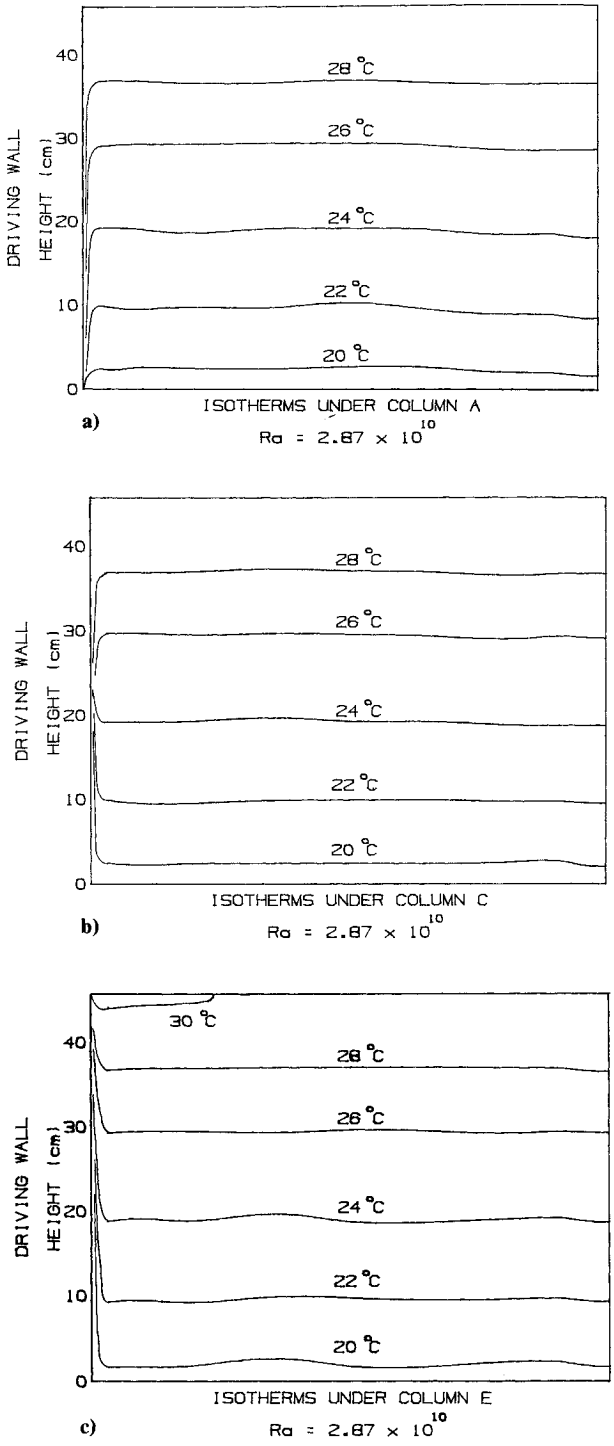

Fig. 5 Isotherm maps for cross sections perpendicular to the driving wall and parallel to the gravity vector; a) isotherms under column A, b) isotherms under column C, and c) isotherms under column E.

shows isotherm maps corresponding to slices parallel to the driving wall. Comparing Figs. 6a–6c, we see by examination of the 30°C isotherm that the warm fluid provided by the driving wall spreads along the top wall. Far away from the driving wall the existence of the warm fluid region is not felt (Fig. 6c). Other than this fact Figs. 6a–6c are remarkably similar and provide additional proof for the result that throughout most of the cavity the temperature field is practically two-dimensional, linearly stratified in the vertical.

The circulation pattern within the cavity became clear with the flow visualization studies described in the previous section. Two boundary layers moved side-by-side on the driving wall,

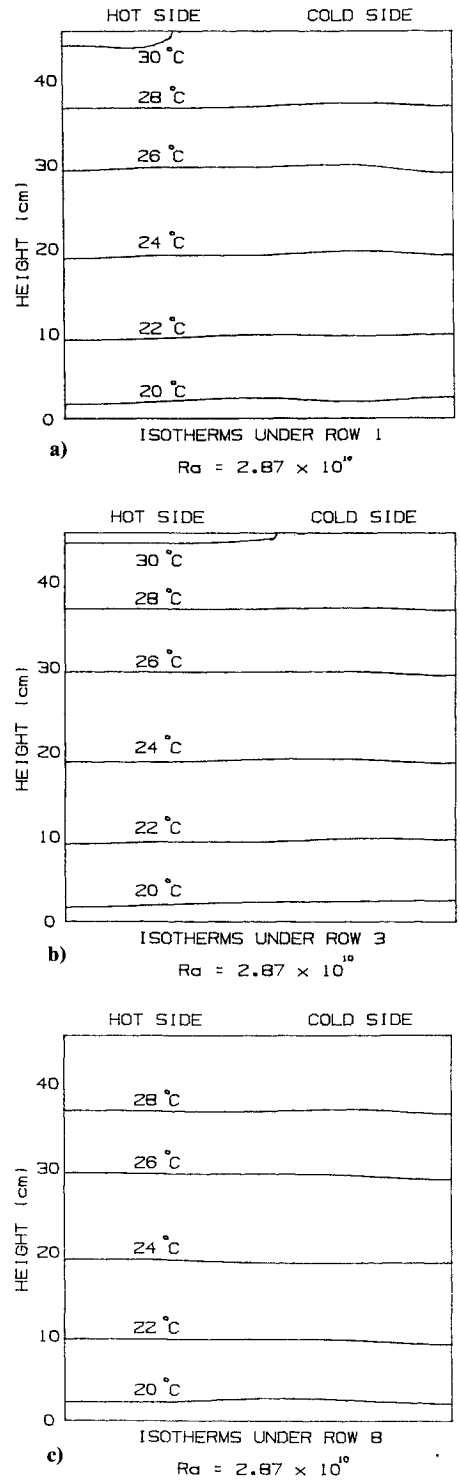

Fig. 6 Isotherm maps for cross sections parallel to the driving wall and parallel to the gravity vector; a) isotherms under row 1, b) isotherms under row 3, and c) isotherms under row 8.

with the warm boundary layer going up and the cool boundary layer moving down at the same rate. The interaction of the two boundary layers was not significant. Repeated observations showed that the two boundary layers were less than 3 mm thick. Fluid flowing up the warm side of the driving wall hits the top wall and creates a turbulent swirl before spreading into a horizontal layer which makes a horseshoe turn (Fig. 7). The momentum of the horizontal layer is such that some fluid cannot complete the turn before crashing into the side wall. Some local turbulence develops, but eventually this fluid returns to the cold wall in a stream following the intersection of the top and side walls. After the turn, the fluid in the top layer flows down the cold wall, spreads in a horizontal layer on the bottom, makes a horseshoe turn similar to the one shown in Fig. 7 and feeds into the warm wall to complete the cycle.

In summary, the temperature and flow fields inside the cavity consist of an "active" region and an "inactive" region. In the active region vivid flow motion renders convection the dominant heat transfer mechanism. The active region occupies a small part of the enclosure: the close vicinity of the driving wall and two thin regions near the horizontal walls. The inactive region constitutes the remainder of the enclosure. In this region heat transfer is conduction dominated.

For each steady state the net heat transfer rate through the enclosure was calculated and is reported in terms of a Nusselt number/Rayleigh number correlation. The definitions used for these two numbers are

$$Nu = \frac{Q}{Wk\,\Delta T} \tag{1}$$

$$Ra = \frac{g\beta H^3\,\Delta T}{\alpha\nu} \tag{2}$$

Q is the sum of the power dissipation in the three heaters. The power to each heater was determined by measuring the voltage drop and resistance across each strip heater. ΔT was taken as the difference of the mean temperatures measured on the warm and cool regions of the driving wall. The fluid properties k, β, α, and ν were taken at the mean temperature of the three thermocouples located in the strip between the warm and cool regions of the wall. Since wall temperatures never exceeded 40°C and the working fluid is water, it is easily shown that radiation effects were negligible compared to overall heat transfer. The correlation for the Nusselt number is

$$Nu = 0.031 \times Ra^{0.324} \qquad (3 \times 10^9 < Ra < 5 \times 10^{10}) \tag{3}$$

The large exponent of Ra in Eq. (3) indicates a strong convective contribution to the overall heat transfer. The fact that the exponent of Ra in Eq. (3) is close to $\frac{1}{3}$ which resembles to what the literature reports for turbulent natural convection from a vertical plate in an infinite isothermal fluid, does not mean that we have turbulent flow in the enclosure. As discussed earlier, the flowfield is, for the most part, laminar. However, the flow configuration in the present problem which yields Eq. (3), is markedly different from the flow configuration for natural convection from a flat plate. Bohn et al.[16] conducted experiments in a cubical enclosure filled with water, in which each wall could be heated or cooled in a controlled manner. Much like in the present study, they found that even at Rayleigh numbers as high as 6×10^{10} the heat transfer mechanism is laminar boundary layer convection, from one wall to the bulk fluid. The flow pattern consisted of boundary layers near the driving walls and an inactive core which did not play an important role on heat transfer. The above findings are in qualitative agreement with the results of the present study.

Scale Analysis

Based on the experimental findings outlined in the previous section, a scale analysis accurate in an order-of-magnitude sense will be developed to explain the heat and fluid flow phenomenon evolving inside the cavity. According to our experimental observations the thermal boundary layers along the warm and the cold regions of the aluminum driving wall are, for all practical purposes, two-dimensional. In addition, the following facts are worth clarifying:

1) The temperature difference between the warm and the cold regions of the driving wall is ΔT ($= T_H - T_C$), Fig. 7.

2) The fluid leaving the warm region of the driving wall is warmer than the cold region of the driving wall by ΔT, Fig. 7.

3) The temperature difference between the cold wall region and the fluid in the stagnant core is θ, with $\theta \leq \Delta T$, Fig. 7.

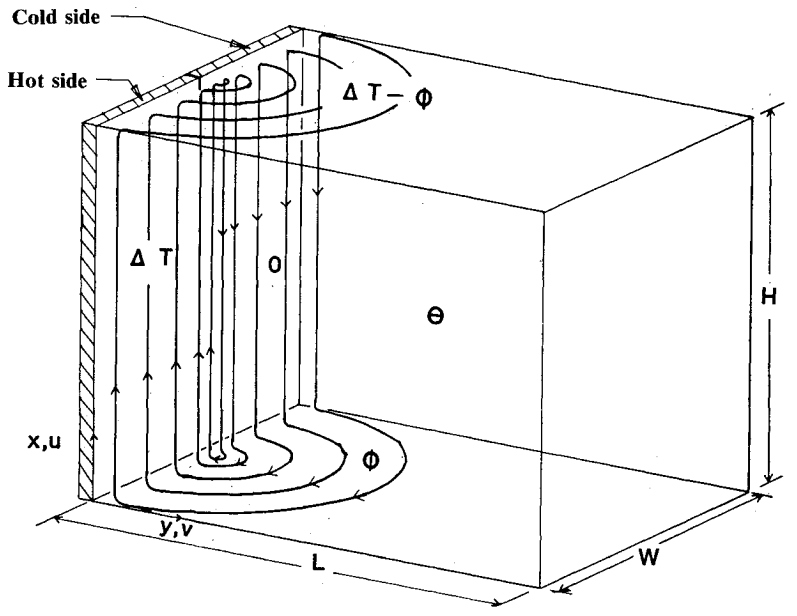

Fig. 7 Artistic interpretation of the flowfield in the enclosure.

4) As the warm fluid leaving the warm region of the aluminum wall starts travelling parallel to the top wall according to the flow pattern in Fig. 7, it loses heat by conduction to the inactive fluid region below it. Therefore, when it reaches the cold part of the aluminum wall and it is ready to start descending, it is driven by a temperature difference *less* than ΔT, namely, $\Delta T - \phi$. The same is true for the cold fluid entering the warm portion of the aluminum wall at the bottom, that is, this fluid gains some heat by conduction from the inactive fluid region above it as it travels along the bottom wall. This heating phenomenon raises its temperature by an amount ϕ (Fig. 7).

The usual steady state Boussinesq-approximated equations governing the conservation of mass, momentum, and energy at each point inside the two-dimensional thermal boundary layer in the vicinity of the warm region of the driving wall are

$$\frac{\partial u}{\partial x} + \frac{\partial v}{\partial y} = 0 \tag{4}$$

$$\frac{\partial}{\partial y}\left(u\frac{\partial u}{\partial x} + v\frac{\partial u}{\partial y}\right) - \frac{\partial}{\partial x}\left(u\frac{\partial v}{\partial x} + v\frac{\partial v}{\partial y}\right) = \nu\left[\frac{\partial}{\partial y}(\nabla^2 u) - \frac{\partial}{\partial x}(\nabla^2 v)\right] - g\beta\frac{\partial T}{\partial x} \tag{5}$$

$$u\frac{\partial T}{\partial x} + v\frac{\partial T}{\partial y} = \alpha\nabla^2 T \tag{6}$$

Note that the two momentum equations were combined into a unique equation [Eq. (5)] by cross-differentiating and subtracting to eliminate the pressure gradient. In addition, the usual Boussinesq approximation accounting for the dependence of density on temperature in the buoyancy term of the momentum equation

$$\rho = \rho_0[1 - \beta(T - T_0)] \tag{7}$$

has been taken into account. It is worth noting that the temperature differences in the fluid during the experiments were small enough for the Boussinesq approximation to be valid.

In the above equations T is the temperature, P the pressure, x and y the Cartesian coordinates, u and v the vertical and horizontal components of velocity, g the gravitational acceleration, and ρ, ν, β, α the fluid density, kinematic viscosity, coefficient of thermal expansion, and thermal diffusivity, respectively. Subscript zero refers to a reference state.

Applying scaling analysis to the momentum [Eq. (5)] and omitting the details for brevity (all the details have been included in Ref. 15) yields

$$\nu\frac{u}{\delta_t^3} \sim g\beta\frac{\Delta T - \theta}{\delta_t} \tag{8}$$

Note that the above relationship represents a balance between friction and buoyancy terms, i.e., the contribution of the inertia terms has been neglected. As it has been shown extensively in the literature[4] this is true for fluids with Prandtl number of order unity or greater. All the symbols for the variables used in the scaling analysis represent the scales corresponding to the real quantities and are defined in the nomenclature.

The energy [Eq. (6)] inside the warm thermal boundary layer requires

$$u\frac{(\Delta T - \phi)}{H} \sim \alpha\frac{\Delta T - \theta}{\delta_t^2} \tag{9}$$

Next we observe that for a steady state condition the energy going into the system through the hot wall, Q_{in}, is the difference between the enthalpy carried by the fluid leaving the hot wall at the top and entering it at the bottom. Thus,

$$Q_{\text{in}} \sim \rho c_p u\frac{W}{2}\delta_t(\Delta T - \phi) \tag{10}$$

This energy entering the cavity must equal the energy leaving the cavity through the cold wall, Q_{out}. $Q_{\text{in}} \sim Q_{\text{out}}$ yields

$$\rho c_p u\delta_t(\Delta T - \phi) \sim kH\frac{\theta}{\delta_t} \tag{11}$$

The final relation needed accounts for the fact that the cooling of the fluid traveling in the region parallel to the top wall from ΔT to $\Delta T - \phi$ is done by conduction through the core, hence,

$$\rho c_p u\delta_t\frac{W}{2}\phi \sim KWL\frac{\Delta T - \phi}{H} \tag{12}$$

Dividing Eqs. (8), (9), (11), and (12) by ΔT yields four equations with the four unknowns u, δ_t, $\theta/\Delta T$, $\phi/\Delta T$.

Solving Eq. (8) for u and recalling the definition of Ra from Eq. (2) we obtain

$$u \sim Ra \frac{\alpha}{H^3} \delta_t^2 \left(1 - \frac{\theta}{\Delta T}\right) \tag{13}$$

Next, taking into account Eqs. (9) and (13)

$$\frac{\delta_t}{H} \sim Ra^{-\frac{1}{4}} \left(1 - \frac{\phi}{\Delta T}\right)^{-\frac{1}{4}} \tag{14}$$

Combining and simplifying Eqs. (12) and (14) produces

$$\frac{1}{2} Ra^{\frac{1}{4}} \left(\frac{\phi}{\Delta T}\right) \left(1 - \frac{\theta}{\Delta T}\right) \left(1 - \frac{\phi}{\Delta T}\right)^{-\frac{7}{4}} \sim \frac{L}{H} \tag{15}$$

Further, by substituting for u from Eq. (13) and δ_t from Eq. (14) into Eq. (11) we can show

$$\frac{\theta}{\Delta T} \sim \frac{1}{2} \tag{16}$$

Substituting this result into Eq. (15) gives

$$\left[\left(\frac{4L}{H}\right)^{-\frac{4}{7}} Ra^{\frac{1}{7}}\right] \left(\frac{\phi}{\Delta T}\right)^{\frac{4}{7}} + \left(\frac{\phi}{\Delta T}\right) - 1 = 0 \tag{17}$$

Finally, combining the definition of Nu, Eq. (1), with Eq. (10) results in

$$\frac{Nu}{f(Ra)} \sim 1 \tag{18}$$

where

$$f(Ra) = \frac{1}{4} Ra^{\frac{1}{4}} \left(1 - \frac{\phi}{\Delta T}\right)^{\frac{1}{4}} \tag{19}$$

Note that in Eq. (19) the temperature difference ϕ is *dependent* on Ra. Therefore, one *should not* conclude that Eqs. (18) and (19) imply that $Nu \sim Ra^{\frac{1}{4}}$. The exact dependence of ϕ on Ra is given in Eq. (17).

To proceed, we solve Eq. (17) numerically for $\phi/\Delta T$ for any given Ra and substitute the result into Eqs. (19) and (18) to find the scale for Nu. The ratio of the experimentally determined Nusselt number divided by $f(Ra)$ is plotted vs Ra in Fig. 8. Clearly, as the scaling predicts, this ratio is of 0(1). In addition, the scaling predicts the correct dependence of Nu on Ra: The ratio of the experimental Nusselt number to the scaling Nusselt number, when plotted against Ra in Fig. 8, is practically independent of Ra. The fact that the simple scale analysis verifies the rather complex picture of the temperature and flow fields painted by our experimental observations adds to the credibility of the findings reported in the study and indicates that scale analysis is a powerful tool which can be used to compliment and explain results obtained by more accurate (in a quantitative sense) methods.

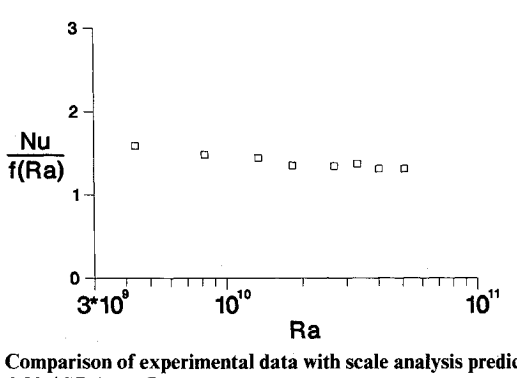

Fig. 8 Comparison of experimental data with scale analysis predictions. Graph of $Nu/f(Ra)$ vs Ra.

Conclusions

This paper reported an experimental and theoretical study of natural convection in a parallelepipedal enclosure driven by a single vertical wall with a warm region adjacent to a cold one. Water was used as the working fluid and the study focused on the high Rayleigh number regime $3 \times 10^9 < Ra < 5 \times 10^{10}$. The following conclusions were drawn.

1) The velocity field in the cavity (Fig. 7) consists of a "ribbon" of fluid which moves up the warm side of the driving wall and makes a horseshoe turn as it spreads across the top wall. It then travels down the cold side of the driving wall and makes a horseshoe turn on the bottom wall to return to the warm side and complete the flow cycle. The remainder of the fluid in the cavity is virtually stagnant. The flow produced by the driving wall penetrates the enclosure only partially. While we are still dealing with a recirculating enclosure flow one should distinguish the present partial penetration flow from flows that occupy the entire enclosure space.

2) The temperature field in the stagnant region is linearly stratified (Figs. 3–6). Sharp thermal boundary layers exist in the vicinity of the driving wall. The temperature field away from the driving wall is remarkably two-dimensional. The three-dimensional part of the temperature field, outside the thermal boundary layer, is limited to two thin and relatively short regions, the one warm in the vicinity of the top wall, and the other cold in the vicinity of the bottom wall. Scale analysis shows that $Nu \sim \frac{1}{4} Ra^{\frac{1}{4}} (1 - \phi/\Delta T)^{\frac{1}{4}}$ where the temperature ratio $\phi/\Delta T$ is a function of Ra. Experimental results yield $Nu \sim 0.031 Ra^{0.324}$. Figure 8 shows these two results to be in excellent agreement indicating the heat transfer model used in the scale analysis accurately reflects the phenomenon inside the cavity.

3) Nonuniformities on the wall temperature, such as the one examined in this paper, may drastically affect the heat and fluid flow characteristics in enclosure natural convection. The resulting temperature and flowfields inside the cavity are markedly different from those of the classical enclosure natural convection model which features two opposite vertical isothermal walls, the one warm and the other cold, and the remaining walls adiabatic.

Acknowledgment

The authors gratefully acknowledge partial support for this research provided by the University of Illinois Research Board and by the National Science Foundation.

References

[1]Churchill, S. W., "Free Convection in Layers and Enclosures," *Heat Exchanger Design Handbook*, edited by E. U. Schlünder, Hemisphere Publishing, Washington, DC, 1983, Chap. 2.5.8.

[2]Catton, I., "Natural Convection in Enclosures," *Sixth International Heat Transfer Conference*, 1978, Vol. 6, 1979, pp. 13–49.

[3]Ostrach, S., "Natural Convection in Enclosures," *Advances in Heat Transfer*, Vol. 8, 1972, pp. 161–227.

[4]Bejan, A., *Convection Heat Transfer*, Wiley, New York, 1984, pp. 159–201.

[5]Poulikakos, D. and Bejan, A., "Natural Convection Experiments in a Triangular Space," *Journal of Heat Transfer*, Vol. 105, 1983, pp. 625–655.

[6]Zebib, A., Schubert, G., and Straus, J., "Infinite Prandtl Number Thermal Convection in a Spherical Shell," *Journal of Fluid Mechanics*, Vol. 97, 1980, pp. 257–277.

[7]Sparrow, E. M., "Laminar Free Convection on a Vertical Plate with Prescribed Nonuniform Wall Heat Flux or Prescribed Nonuniform Wall Temperature," NACA TN 3508, 1955.

[8]Schetz, J. A. and Eichhorn, R., "Natural Convection with Discontinuous Wall-Temperature Variations," *Journal of Fluid Mechanics*, Vol. 18, Part 2, 1964, pp. 167–175.

[9]Jaluria, Y., "Buoyancy-Induced Flow Due to Isothermal Thermal Sources on a Vertical Surface," *Natural Convection*, edited by I. Catton and R. N. Smith, American Society of Mechanical Engineers, Heat Transfer Division, Vol. 16, 1981, pp. 25–33.

[10]Chao, P. K. B., Ozoe, H., Churchill, S. W., and Lior, N., "Laminar Natural Convection in an Inclined Rectangular Box with the Lower Surface Half-Insulated," *Journal of Heat Transfer*, Vol. 105, 1983, pp. 422–432.

[11]Chao, P. K. B., Ozoe, H., and Churchill, S. W., "The Effect of a Nonuniform Surface Temperature on Laminar Natural Convection in a Rectangular Enclosure," *Chemical Engineering Communications*, Vol. 9, 1981, 245–254.

[12]Filis, P. and Poulikakos, D., "An Experimental Study on the Effects of Wall Temperature Nonuniformity on Natural Convection in an Enclosure Heated from the Side," *International Journal of Heat and Fluid Flow*, Vol. 7, 1986, pp. 258–265.

[13]Poulikakos, D., "Natural Convection in a Confined Fluid-Filled Space Driven by a Single Vertical Wall with Warm and Cold Regions," *Journal of Heat Transfer*, Vol. 107, 1985, pp. 867–876.

[14]Humphrey, J. A. C. and Bleinc, C., "On the Structure of the Flow Due to the Collision of Opposed, Vertical, Free Convection, Boundary Layers," *International Communications in Heat and Mass Transfer*, Vol. 12, 1985, pp. 233–240.

[15]Sadowski, D., "Three-Dimensional Natural Convection Experiments in a Cavity Driven by a Single Wall with a Warm and a Cold Region," M.S. Thesis, Dept. of Mechanical Engineering, Univ. of Illinois, Chicago, IL, 1986.

[16]Bohn, M. S., Kirkpatrick, A. T., and Olson, D. A., "Experimental Study of Three-Dimensional Natural Convection High-Rayleigh Number," *Journal of Heat Transfer*, Vol. 106, 1984, pp. 339–345.